Research papers

A progressive segmented optimization algorithm for calibrating time-variant parameters of the snowmelt runoff model (SRM)

Shunping Xie[a,b], Jinkang Du[a,b,*], Xiaobing Zhou[c], Xueliang Zhang[a], Xuezhi Feng[a], Wenlong Zheng[a], Zhiguang Li[a], Chong-Yu Xu[d]

[a] School of Geography and Ocean Science, Nanjing University, Nanjing, China
[b] Jiangsu Center for Collaborative Innovation in Geographical Information Resource Development and Application, Nanjing, China
[c] Department of Geophysical Engineering, Montana Tech of The University of Montana, Butte, MT 59701, USA
[d] Department of Geosciences, University of Oslo, PO Box 1047 Blindern, N-0316 Oslo, Norway

ARTICLE INFO

ABSTRACT

To capture the temporal variability of parameters of hydrological models, the segmented optimization algorithm (SOA) is usually used which subdivides the calibration period into a number of sub-periods and seeks optimal parameters for each sub-period by optimizing the objective function based on the measured and estimated data in the same sub-period. In this paper, we developed a new method that is called a progressive segmented optimization algorithm (PSOA), which seeks optimal parameters by optimizing the objective function based on both the current and all the prior sub-periods.

We applied and compared the SOA and PSOA algorithms to the Snowmelt Runoff Model (SRM) in simulating snow-melt streamflow for the Manasi River basin, northwest of China, during snowmelt seasons of 2001–2012. The study showed: (1) PSOA can effectively calibrate the time-variant model parameters while avoiding too much computational time caused by a significant increase of parameter dimensionality. (2) PSOA outperforms SOA for both single-snowmelt-season and multi-snowmelt-season simulations. (3) For single-snowmelt-season simulation, the length of the sub-period has an apparent effect on model performance, the shorter the sub-period is, the better the model performance will be, when the model is calibrated using the PSOA method. (4) For multi-snowmelt-season simulation, an over-short sub-period may cause overfitting problems in some cases such as the situation of taking Nash-Sutcliffe efficiency (NSE) as the objective function. A compromised length of sub-period and objective function may have to be chosen as a trade-off among evaluation criteria and between the importance of calibration and validation.

1. Introduction

Model calibration, which attempts to estimate values of some critical model parameters that are not usually available or cannot be physically measured, is one of the main research topics in the application of hydrological models to real case simulations (Gupta and Sorooshian, 1983; Beven and Binley, 1992; Shamir et al., 2005). The classical single-objective approaches primarily focus on matching one aspect of the hydrograph, but other important hydrological processes implicit in the observations cannot be captured simultaneously (Boyle et al., 2000). The multi-objective approaches take into consideration of different aspects of the hydrograph by accounting for the trade-off among different performance indicators (Gupta et al., 1998; Yapo et al., 1998; Boyle et al., 2000; Madsen, 2000; Vrugt et al., 2003; Jie et al.,

2016), which not only allow for an analysis of the trade-offs among the different objective functions but also enable hydrologists to better understand model structures (Zhou et al., 2014; Jie et al., 2016).

The rainfall-runoff processes are very complex due to a large number of controlling factors. Some factors such as climatic conditions and land use/land covers vary in time, leading to a time-varying nature of hydrological responses over different temporal scales, e.g. annual, seasonal, monthly and daily scales (Beighley and Moglen, 2002; Merz et al., 2006; Choi and Beven, 2007; Zhang et al., 2011; Tian et al., 2012; Hao et al., 2015).

The dynamic nature of hydrological systems brings uncertainties into hydrological simulations and predictions, posing a challenge to accurate prediction/forecasting of streamflow. Previous studies have shown that hydrological processes switch their dynamics between time

steps/periods, which have not been properly represented by the existing models, and dynamic calibration of the time varying hydrological processes will improve the prediction or forecasting ability of the hydrological models (Choi and Beven, 2007; Levesque et al., 2008; Zhang et al., 2011; Kim and Lee, 2014; Kim, 2016; Chen et al., 2018).

The most commonly used approach in the dynamic calibration of the time varying hydrological processes is to divide the whole calibration time period (e.g. hydrological year and snowmelt season) into several sub-periods of hydroclimatic similarity, and assume that the model parameters are constant in each sub-period. For example, Hay et al. (2009) divided the hydrologic year into three groups based on an atmospheric pressure index. Kim and Lee (2014) divided the calibration period into four seasons based on seasonal rainfall and streamflow patterns; Paik et al. (2005) divided the calibration period into three 4-month seasons (i.e. warm and dry, rainy, and cold and dry). Zhang et al. (2015a,b), Kim (2016) and Chen et al. (2018) separated the calibration period into dry and wet periods. To improve model performance, some researchers divided the calibration period into sub-periods using clustering methods based on similar characteristics in the data during the model calibration period, such as the Fuzzy C-mean Clustering method (Choi and Beven, 2007; Zhang et al., 2011), the traditional k-means clustering algorithm (de Vos et al., 2010), and the Self-Organizing Maps based clustering method (Toth, 2009).

Dividing a calibration period into too many sub-periods leads to a significant increase in the parameter dimension, making parameter calibration much more complex and time consuming. To overcome the difficulties, a feasible approach has been developed that calibrates parameters independently for each sub-period which is referred to as segmented optimization algorithm (SOA). However, SOA only optimizes parameters of each sub-period to match the observed data just for that sub-period and not for the whole period. Hence, the optimized parameters of each sub-period may not be globally optimal. In view of the drawback of SOA, we proposed a progressive segmented optimization algorithm (PSOA) for calibrating time-variant parameters of hydrological models by dividing the calibration period into several sub-periods and optimizing those parameters of each sub-period to match the observed data of the whole period. With such an approach, global solution of parameters for all sub-periods is obtained consequently and progressively. To test the effectiveness of PSOA compared to SOA, we took Snowmelt Runoff Model as an example to simulate snowmelt runoff process with the time-variant parameters in the Manasi River basin, Northwest China.

The main parts of the paper are organized as follows. The geographical and hydrological characteristics of the study area, including the data sources and data preprocessing are described in Section 2. The SRM model and the proposed calibration algorithm are explicated in Section 3. The results and discussions about possible effects of objective functions and sub-period length on model outputs are presented in Sections 4 and 5. Conclusions are presented in Section 6.

2. Study area and data

2.1. Study area

The Manasi River basin (43°05′N-44°10′N and 85°00′E-86°20′E), which is located in the Xinjiang Uygur Autonomous Region, Northwest China, has a total area of 5179 km² above the Kensiwate (KSWT) Station (see Fig. 1). The Manasi River basin is one of the biggest irrigation areas in China. The Manasi River, about 400 km long, originates in the northern slope of Tianshan Mountains, and it is the longest inland river in the Junggar Basin. Land covers in the Manasi River basin take the form of bare soil, open shrub lands, grassland, wood/grassland, meadow, and snow/ice.

The Manasi River basin has a typical temperate continental arid climate. The elevation of the basin ranges from 500 to 5216 m above mean sea level (a.m.s.l.), and the difference in height within the basin results in significant uneven distributions of temperature and precipitation. The mean annual air temperature ranges from below 0 °C in the mountainous areas to approximately 9 °C at the basin outlet. Precipitation is abundant within the area of elevation between 1500 m and 3600 m, where the mean annual precipitation reaches 600–700 mm, but it drops to 100–200 mm in the piedmont plain (Feng et al., 2000; Ji and Chen, 2012). Precipitation occurs mainly in summer (June, July, and August) and less in winter (December, January, and February) in the form of snowfall. Snow accumulates in winter and ablates mainly in spring and early summer (June), and it completely disappears in late summer.

The average annual runoff is about $12.8 \times 10^8 \, \text{m}^3$, the intra-annual distribution of runoff is uneven, with about 9.7, 69.8, 16.5, and 5.0% of the annual runoff occurring in spring (March–May), summer, autumn (September–November), and winter, respectively. Meltwater from snow and glaciers in the spring and summer months accounts for about 35.9% of the annual runoff (Feng et al., 2000). Groundwater flow accounts for a small percentage of the total runoff but it dominates the streamflow in winter when there is neither rainfall nor meltwater. For simplicity, meltwater due to snow and glaciers will not be distinguished in the following discussion, because runoff from meltwater of glaciers mainly happens in summer and geographically limited only to a small scale.

There are four hydrological stations at the lower part of the basin: Meiyao (MY), Kensiwate (KSWT), Qingshuihezi (QSHZ), and Hongshanzui (HSZ). The HSZ Station has been abandoned since 2006. To take advantage of the observed data at the other three stations, the study area is thus taken as the portion of the basin above the KSWT Station as is shown in Fig. 1. The geographical and hydro-climatic characteristics of the three stations are listed in Table 1.

2.2. Data sources

The digital elevation model (DEM) used in this study is the Shuttle Radar Topography Mission (SRTM) data, with the resolution of 90 m (Farr et al., 2007). The SRTM data were downloaded from http://srtm.csi.cgiar.org/. The DEM data were used for altitudinal belt partition, zonal area estimation, and temperature and precipitation interpolation.

Daily precipitation and air temperature data observed at the MY, KSWT, and QSHZ hydrological stations (Fig. 1) from 2001 to 2012 were used as model inputs. Daily runoff data from 2001 to 2012 at the KSWT Station were used for model calibration and verification. The data were obtained from Manasi Hydrological Bureau. The hydro-meteorological network is very sparse and the three hydrological stations are at the proximity to the basin outlet, data from this network can hardly represent the daily rainfall distribution at the basin level. Thus, the daily precipitation at different elevation zones was estimated through synthetization of the observations at the three hydrological stations with the relative annual precipitation gradient derived from corrected Tropical Rainfall Measuring Mission (TRMM) data based on the regression models for the same study area as was discussed by Ji and Chen (2012).

As there is no operational snow monitoring system established in the study area, the MODIS snow cover data were used for model simulation. Numerous SRM applications have had success in using snow data from MODIS (Butt and Bilal, 2011; Georgievsky, 2009; Immerzeel et al., 2009; Qiu et al., 2013; Tahir et al., 2011). For these studies conducted in watersheds with size between 500 and 27,000 km², the 500 m resolution of MODIS was found sufficient for estimating the fraction of snow covered area (Kult et al., 2014). The MODIS 8-day composite snow cover data product (MOD10A2) has higher precision in snow classification than MODIS daily products (Zhou et al., 2005; Huang et al., 2007). In this study we adopted the MODIS 8-day composite product MOD10A2 from March to June during 2001 to 2012 to derive the fraction of snow-covered area for each zone. The missing data (2 scenes are missing) were obtained by a linear spatial interpolation algorithm, assuming that the change with time between two
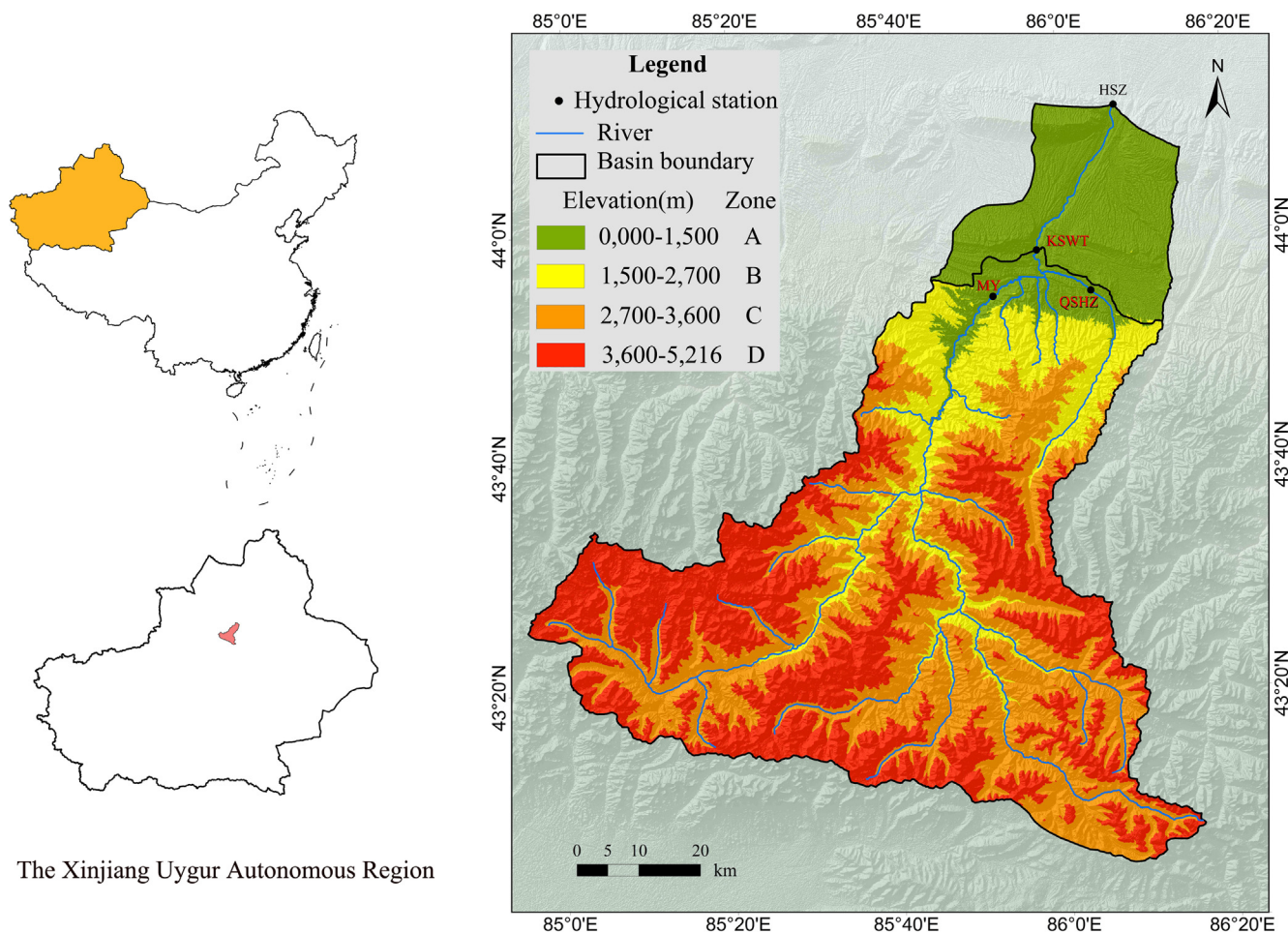
Fig. 1. The boundary, river network, hydrological stations (Kensiwate-KSWT, Meiyao-MY, Qinshuihezi-QSHZ, Hongshanzui-HSZ), and four elevation zones of the study area.

consecutive "8-day" snow fractions is linear. The daily snow fraction of any date between the two "8-day" periods for each zone is also calculated by linear spatial interpolation algorithm.

The detailed information about the data is summarized in Table 2. The daily precipitation at stations MY, QSHZ, and KSWT is the total precipitation of rainfall and snowfall, there is no detailed information on whether the total precipitation on a specific day is snow or rainfall.

3. Methodology

3.1. Snow runoff model (SRM)

SRM is a conceptual, semi-distributed, and degree-day (temperature index) model developed by Martinec (1975). It has been used to simulate, predict, and/or forecast daily runoff resulting from snowmelt

Table 2
Information of the datasets used in this study.

Data	Unit	Sources	periods	location
Daily precipitation	mm	local hydrological bureau	2001–2012	MY, QSHZ, KSWT
Daily Temperature	°C	Same as above	2001–2012	MY, QSHZ, KSWT
Daily runoff	m³/s	Same as above	2001–2012	KSWT
DEM	m	http://srtm.csi.cgiar.org/SELECTION/inputCoord.asp		All basin
MOD10A2	m	https://nsidc.org/data/MOD10A2	2001–2012	All basin

Table 1
The geographical and hydro-climatic characteristics of the hydrological stations within Manasi River basin from Manasi Hydrological Bureau. * the annual precipitation in MY Station was obtained from observation period of 1978–2005.

Station	Longitude/Latitude	Elevation (m.a.m.s.l)	Control area (km²)	Annual precipitation (mm)	Maximum instantaneous flow (m³/s)	Annual runoff (mm)	Period of hydro-climatic statistics
Kensiwate (KSWT)	85°57′19″E/43°58′14″N	940	5179	339	1100	238	1957–2005
Meiyao (MY)	85°51′49″E/43°54′34″N	1300	3902	384*	822	261	1954–2005
Qingshuihezi (QSHZ)	86°3′42″E/43°54′53″N	1320	437	430	96	298	1980–2005

and rainfall in mountainous regions, and has been tested for over 100 basins at different geographical locations and spatial ranges in 29 countries (Martinec et al., 2008). Model input variables include daily average air temperature, daily total precipitation, and snow cover area. Based on the input values, the following equation is used in SRM to calculate the daily streamflow Q (m^3/s):

$$Q_{i+1} = Q_i k_{i+1} + \frac{10000}{86400}(1-k_{i+1}) \sum_l (C_{Sl,i} \times a_{l,i}(T_i + \Delta T_{l,i})S_{l,i}$$
$$+ C_{Rl,i} \times P_{l,i})A_l \tag{1}$$

where i is the day number ($i = 1,…, N$, N is the total number of days), Q_1 is the observed initial value of daily streamflow value before the simulation begins. l is the index for each elevation zone ($l = 1,…, L$, L is the total number of elevation zones). 10000/86400 is the conversion factor from cm km^2 day^{-1} to m^3 s^{-1}, k is the recession coefficient. Corresponding to the l-th elevation zone, C_S and C_R are the runoff coefficients expressing the losses as a ratio of runoff contributed by snowmelt and rain to precipitation, respectively, of the elevation zone. a is the degree-day factor (cm $^\circ$C^{-1} d^{-1}), T is the number of degree-days of station ($^\circ$C d), ΔT is the adjustment by temperature lapse rate when extrapolating the temperature from the station to the average hypsometric elevation of the zone ($^\circ$C d), S is the fraction of snow covered area (%), P is the precipitation contributing to runoff (cm), and A_l is the area of elevation zone l (km^2).

3.2. Determination of input variables and parameters

SRM is set up with daily input data of air temperature, precipitation, and fraction of snow covered area. The basin was divided into four altitudinal zones with a nearly 1000 m difference in hypsometric elevation between each two neighboring zones. The elevation boundaries, areas, land covers of each zone are detailed in Table 3.

3.2.1. Daily zonal mean temperature

The daily zonal mean temperatures were determined by extrapolating the mean temperature records available at the three hydrological stations by using the lapse rate value. The temperature adjusted ΔT through temperature lapse rate is computed as follows:

$$\Delta T = \gamma (h_{st}-h)\frac{1}{100} \tag{2}$$

where γ is the temperature lapse rate ($^\circ$C/100 m), h_{st} is the altitude of the hydrological station where temperature was measured, h is the hypsometric mean elevation of a zone (m).

Studies in various high mountain catchments have shown spatial and temporal variability of the temperature lapse rate (Tahir et al., 2011; Zhang et al., 2015a,b). Due to the lack of observed data in the area, those values were determined based on the study over the same area by Feng et al. (2000) (Table 4). Since the difference in height among the observed sites is as large as 400 m, validation of those values using observed data is not possible due to lack of observed temperature in higher elevation resolution. However, from Table 4 we can see that except for the lowest Zone A, the temperature lapse rate increases from March to June in all other zones. In March, the temperature lapse rate increases with elevation (from 0.50 $^\circ$C/100 m for Zone A to 0.64 $^\circ$C/100 m for Zone D), while in April the temperature lapse rate remains almost constant (0.64–0.65 $^\circ$C/100 m). In May, the temperature lapse

Table 3
Definition, areas and land covers of the four zones.

Zone	A	B	C	D
Elevation (m a.m.s.l)	< 1500	1500–2700	2700–3600	> 3600
Area (km^2)	250	804	2114	2011
Land cover	Desert steppe	spruce forest	alpine meadow	snow/ice

Table 4
The temperature lapse rate ($^\circ$C/100 m) in the study region.

Zone	March	April	May	June
A	0.50	0.64	0.78	0.77
B	0.55	0.65	0.75	0.77
C	0.60	0.65	0.73	0.78
D	0.64	0.65	0.70	0.72

rate decreases with elevation (from 0.78 $^\circ$C/100 m for Zone A to 0.70 $^\circ$C/100 m for Zone D). In June, Zones A–C show almost constant temperature lapse rate (0.77–0.78 $^\circ$C/100 m), but decreases to 0.72 $^\circ$C/100 m in the highest zone (Zone D). The spatial and temporal variability of the temperature lapse rate within these zones may indicate the local climate conditions of the basin.

3.2.2. Critical temperature

A critical temperature T_C is used to decide whether a precipitation event is treated as rainfall or snowfall. The critical temperature is usually higher than freezing point and diminishes to 0 $^\circ$C as snowmelt season progresses. According to meteorological observations at the Tianshan Snow Observation Station, the critical temperature from the beginning to the end of the snowmelt season was observed to decrease from 3.5 to 0 $^\circ$C (Xu, 1996). Since the Tianshan Snow Observation Station and the Manasi River basin are both located in Tianshan Mountain and they are about 100 km apart, we took the daily T_C values from 3.5 $^\circ$C to 0 $^\circ$C for the beginning to the end of a snowmelt season for each zone. The times for the beginning and the end of the snowmelt season of each zone in the study area are determined based on the averaged snow ablation curve of multiple years for each zone and they are listed in Table 5. The daily T_C value for the beginning and the end of each snowmelt season was set to be 3.5 $^\circ$C and 0 $^\circ$C, respectively. The daily T_C value for any day in between was interpolated linearly from 3.5 $^\circ$C to 0 $^\circ$C.

3.2.3. Precipitation

The precipitation in each zone was estimated by synthesizing the observed data at the three hydrological stations with the precipitation gradient. Since no precipitation data are available for the area with the altitudes above 2000 m, and vertical distribution of the precipitation is uneven (Hu, 2004; Ji and Chen, 2012), the precipitation gradient cannot be estimated from the rain-gauge observations alone which are located at downstream. Ji and Chen (2012) found the annual precipitation gradient in the area was 14.3 mm/100 m for Zone B, −8.1 mm/100 m for Zone C, and 6.6 mm/100 m for Zone D based on the corrected Tropical Rainfall Measuring Mission (TRMM) data for the period of 1998 to 2009. In this study, the daily precipitation in Zone A was taken as the average of the observations at the three hydrological stations; in other zones, they were estimated using the relative precipitation gradients based on the annual precipitation gradient (Ji and Chen, 2012) and the base value of the daily precipitation in Zone A, the daily precipitation in Zone l is computed as follows:

$$P_l = P_A + d_l h_l \tag{3}$$

where P_A is the daily precipitation in Zone A, P_l and h_l are the daily precipitation and altitude, respectively, in Zone l ($l = B, C,$ or D), d_l is

Table 5
The beginning and end times of snowmelt season in different zones.

Zone	The beginning time	The end time
A	the 20th of March	the 10th of May
B	the 10th of April	the 30th of May
C	the 30th of April	the 30th of June
D	the first of June	the 20th of August

Table 6
The mass density of snow in different months and zones (g/cm³).

Zone	March	April	May	June
A	0.20	0.24	0.31	0.33
B	0.20	0.23	0.30	0.32
C	0.19	0.22	0.29	0.31
D	0.19	0.22	0.29	0.31

the relative precipitation gradient of Zone *l* to Zone A.

Precipitation contribution to runoff is considered in SRM according to different stages of snowmelt season. If the air temperature is lower than the critical temperature, the precipitation is treated as new snow. The new snowfall over the snow-free area is considered as precipitation to be added to snowmelt calculation. Otherwise, if the air temperature is above the critical temperature, the precipitation as rainfall within the area of the entire zone is added (Martinec et al., 2008).

3.2.4. Degree-day factor

The degree-day factor was obtained from an empirical relation (Martinec and Rango, 1986):

$$a = 1.1 \frac{\rho_s}{\rho_w} \tag{4}$$

where ρ_s is the mass density of snow and ρ_w the mass density of water that was set to be 1 g/cm³. The density of snow increases as the melt season progresses from winter to summer and the snowpack becomes wetter and denser. By referring to the *in situ* data of ρ_s in the Tianshan Mountain (Hu, 2004), ρ_s values were set for different zones from March to June (Table 6).

3.2.5. Runoff and recession coefficients

The runoff coefficients for rainfall and snowfall (C_R and C_S) at a daily scale increase from lower to higher elevation zones, given other factors such as soil and topography unchanged, as warmer temperatures result in higher losses from evapotranspiration or sublimation. In this study, C_S and C_R in the zone A were calibrated as the season progresses, and were set to increase by 10% per zone in other zones, which produced the best results by using the trial-and-error calibration method.

The recession coefficient *k* indicates the decline of discharge in a period without snowmelt or rainfall. Corresponding to the ratio of runoff on consecutive days without snowmelt and rainfall, *k* is assumed to vary with discharge Q as (Martinec et al., 2008):

$$k_{i+1} = \frac{Q_{i+1}}{Q_i} = \rho Q_i^{-\sigma} \tag{5}$$

where i, $i + 1$ are the sequence of days during a true recession flow period. ρ and σ are parameters. Eq. (5) can be reformatted by taking the natural log on both sides of the equation as:

$$\ln(Q_{i+1}) = \omega + \varphi \ln(Q_i) \tag{6}$$

where $\omega = \ln(\rho)$ and $\varphi = 1 - \sigma$. Parameters ω and φ in Eq. (6) can be obtained through linear regression analysis using the observed discharge data.

In summary, due to the non-uniformity of snowmelt runoff process throughout the snowmelt season, some parameters (temperature laps rate, snow density, runoff coefficients, etc.) of snowmelt runoff model should vary with time to reflect the time-varying characteristics of the runoff response mechanisms. The temperature lapse rate and snow density were set to vary monthly over different elevation zones, the critical temperatures were set to vary daily, and their values were determined in advance (Tables 4–6). The runoff coefficients of snowmelt and rainfall were also allowed to vary for different length of sub-periods such as one month, half a month, ten days, and five days; they need to be calibrated since they are not measurable by definition and can't be estimated simultaneously with runoff.

3.3. Calibration algorithm

3.3.1. The segmented optimization algorithm (SOA) algorithm

The SOA algorithm separates the calibration period (e.g. hydrological year) into several sub-periods (e.g. four seasons) (Kim and Lee, 2014). The model parameters to be calibrated in different sub-periods are assumed to be independent of each other. Optimization is then performed consecutively and independently in one sub-period followed by the next till the last one. The objective function for each sub-period is built upon the observed and simulated data of that period. Any known optimization method can be used in each sub-period. The procedure of SOA is shown in Table 7 and Fig. 2. Supposing there is only one time-varying parameter β, and the whole period is divided into n sub-periods with the same length of m (e.g. if one year is divided into 12 months, each month has a length of 30 days on average, then n = 12, m = 30), in each sub-period there are m observed runoff records. Then the total observed runoff series in the whole period can be expressed as: $O_1, O_2, …, O_{nm}$. Similarly, the total simulated runoff series can be expressed as: $S_1, S_2, …, S_{nm}$ corresponding to the β values. The objective of calibration is to find the best value of β for each sub-period denoted by $β_1, β_2,…, β_n$, making objective function $f()$ optimal. The simulated runoffs in each sub-period i are dependent on $β_i$. The calibration can be implemented through n steps. In each step, the $β_i$ is optimized with the objective function built upon the observed and simulated runoff series of sub-period i.

The SOA algorithm optimizes model parameters of each sub-period independently. The drawback of such a method is that the parameters are optimized just based on the observed and simulated runoff of the current sub-period rather than the whole calibration period.

3.3.2. The progressive segmented optimization algorithm (PSOA) algorithm

To overcome the shortcoming of SOA mentioned above, we propose PSOA to optimize parameters. The procedure of PSOA includes two phases (Table 8 and Fig. 3). In the first phase, the parameters of the
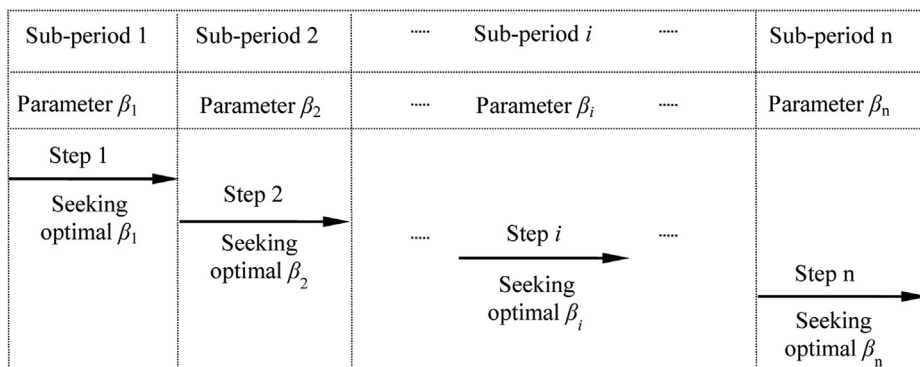
Table 7
The procedure of SOA.

Sub-period No.	1	2	…	n
Parameters	$β_1$	$β_2$	…	$β_n$
Observed runoff series	$O_1, …, O_m$	$O_{1+m}, …, O_{2m}$	…	$O_{1+(n-1)m}, …, O_{nm}$
Simulated runoff series	$S_1, …, S_m$	$S_{1+m}, …, S_{2m}$	…	$S_{1+(n-1)m}, …, S_{nm}$
Step1: Seeking optimal $β_1$	$\underset{β_1}{\text{Opt}} \begin{cases} f(O_1,...,O_m, \\ S_1, … , S_m) \end{cases}$			
Step2: Seeking optimal $β_2$		$\underset{β_2}{\text{Opt}} \begin{cases} f(O_{1+m},...,O_{2m}, \\ S_{1+m}, … , S_{2m}) \end{cases}$		
Stepn: Seeking optimal $β_n$				$\underset{β_n}{\text{Opt}} \begin{cases} f(O_{1+(n-1)m},...,O_{nm}, \\ S_{1+(n-1)m}, …, S_{nm}) \end{cases}$

Fig. 2. A sketch of processing flow of the SOA algorithm. The top row is the series of sub-periods. The second row from the top is the corresponding series of parameters to be optimized. The other rows represent the process of optimization during the specific sub-period. The length of arrow in step i represents the number of sub-periods during which the observed and simulated runoffs are used to find optimal solutions of parameter β_i.

model in each sub-period are optimized separately through n steps from sub-period 1 to sub-period n. In step 1, the β_1 is optimized with the objective function built upon the observed and simulated runoff series of sub-period 1. In step 2, the β_2 is optimized with the objective function built upon the observed and simulated runoff series of sub-period 1 and sub-period 2. Accordingly, in step n, the β_n is optimized with the objective function built upon the observed and the simulated runoff series of sub-period 1 to sub-period n, the simulated runoff series of sub-period 1 to sub-period n-1 are the results of hydrological model simulation based on optimized β_1 to β_{n-1}. In this way, the parameter optimization of the current sub-period takes into account the results of the optimized parameters of all the previous sub-periods.

In the second phase, the parameters of the model are still optimized successively through n steps from sub-period 1 to sub-period n. In step i, the β_i is optimized with the objective function built upon the observed and simulated runoff series of all the sub-periods, in which the simulated runoff series of sub-periods 1 to $i-1$, and sub-periods $i+1$ to n are from the most lately simulated results. The calibration in the second phase will be repeated until the improvement of the whole objective function is less than a given tolerance. The characteristic of the calibration in the second phase is that the parameters of each sub-period are globally optimized after recursive optimization. In such a way, the shortcomings in the calibration of time-varying parameters using the SOA method can be overcome. As far as we know, there is no similar method in the literature.

3.4. The model evaluation criteria

In order to evaluate statistically the accuracy of the calibrated and validated runoff outputs using the new calibration method, different parts of the hydrograph should be considered with the appropriate evaluation criteria. Low and high flows need to be simulated well and a good mass balance is also required. In this study, the following three commonly used criteria were employed: the Nash-Sutcliffe efficiency (NSE), the NSE_{ln} (the NSE calculated using log-transformed discharge) and volume difference (Dv).

NSE is given by (Nash and Sutcliffe, 1970)

$$NSE = 1 - \frac{\sum_{i=1}^{n}(O_i - S_i)^2}{\sum_{i=1}^{n}(O_i - O)^2} \tag{7}$$

and NSE_{ln} is given by

$$NSE_{ln} = 1 - \frac{\sum_{i=1}^{n}(lnO_i - lnS_i)^2}{\sum_{i=1}^{n}(lnO_i - lnO)^2} \tag{8}$$

where O_i is the observed daily discharge, S_i is the simulated daily discharge, if O_i or S_i is equal to 0, it should be set to a small positive value less than 1. O is the average observed discharge, and i is the day number, $i = 1, \ldots, n$, where n is the total number of daily discharge records.

The Dv (%) is given by

$$Dv = \frac{V - V'}{V} * 100 \tag{9}$$

where V is the observed runoff volume and V' is the simulated runoff volume.

NSE has been widely employed to evaluate the performances of hydrological models, and it tends to emphasize the high or peak flows.

Table 8
The procedure of PSOA.

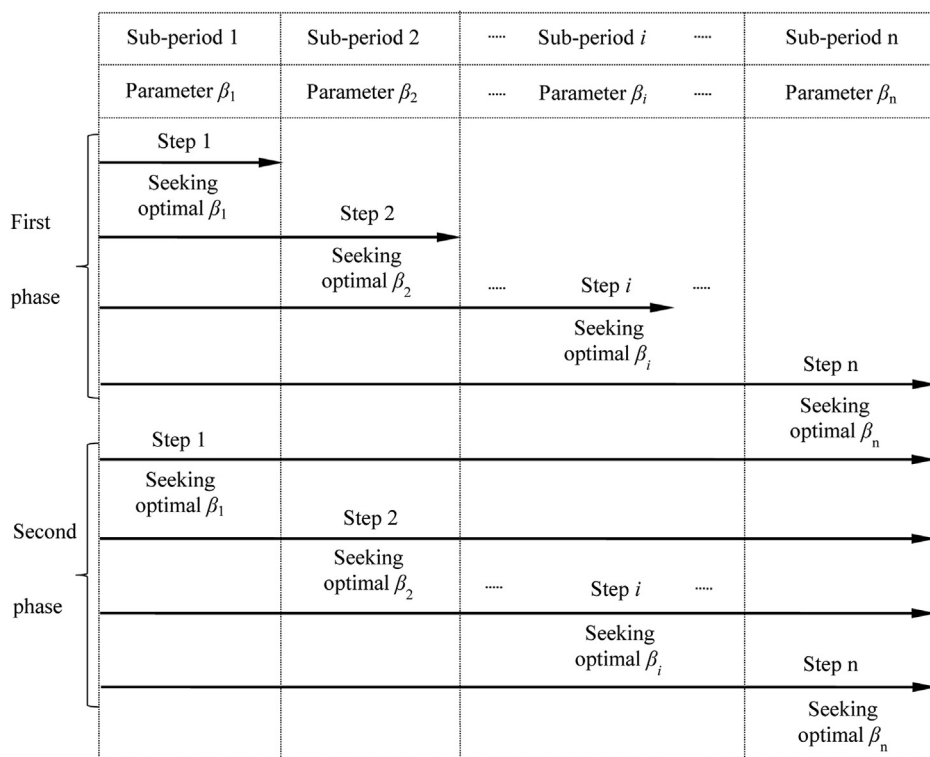|		1	2	...	N
Sub-period No.		1	2	...	N
Parameters		β_1	β_2	...	β_n
Observed runoff series		$O_1, \ldots, O_m$	$O_{1+m}, \ldots, O_{2m}$	...	$O_{1+(n-1)m}, \ldots, O_{nm}$
Simulated runoff series		$S_1, \ldots, S_m$	$S_{1+m}, \ldots, S_{2m}$	...	$S_{1+(n-1)m}, \ldots, S_{nm}$
First phase	Step1: Seeking optimal β_1	$\underset{\beta_1}{Opt}\begin{cases} f(O_1,\cdots,O_m, \\ S_1,\cdots,S_m) \end{cases}$			
	Step2: Seeking optimal β_2		$\underset{\beta_2}{Opt}\begin{cases} f(O_1,\cdots,O_{2m}, \\ S_1,\cdots,S_{2m}) \end{cases}$		
	Stepn:Seeking optimal β_n				$\underset{\beta_n}{Opt}\begin{cases} f(O_1,\cdots,O_{nm}, \\ S_1,\cdots,S_{nm}) \end{cases}$
Second phase	Step1: Seeking optimal β_1	$\underset{\beta_1}{Opt}\begin{cases} f(O_1,\cdots,O_{nm}, \\ S_1,\cdots,S_{nm}) \end{cases}$			
	Step2: Seeking optimal β_2		$\underset{\beta_2}{Opt}\begin{cases} f(O_1,\cdots,O_{nm}, \\ S_1,\cdots,S_{nm}) \end{cases}$		
	Step n: Seeking optimal β_n				$\underset{\beta_n}{Opt}\begin{cases} f(O_1,\cdots,O_{nm}, \\ S_1,\cdots,S_{nm}) \end{cases}$

Fig. 3. A sketch of processing flow of the PSOA algorithm. The top row is the series of sub-periods. The second row from the top is the corresponding series of parameters to be optimized. The rows in the first phase is the process of optimization in the first phase for each sub-period. The difference of the PSOA algorithm from the SOA algorithm during this phase is that optimization in the step i considers all previous sub-periods. The rows in the second phase represent the process of optimization of parameter corresponding to each sub-period during the second phase within the whole calibration period (sum of all the sub-periods). The length of arrow in step i represents the number of sub-periods during which the observed and simulated runoffs are used to find optimal solution of parameter β_i.

NSE_{ln} places more emphasis on fitting low flows (Chen et al., 2018). The Dv is a measure of the average deviation between the simulated and observed volumes.

From a multi-objective viewpoint, all criteria could not reach their best values simultaneously, a balanced, compromised, aggregated evaluation considering different criteria should be made. In this study, the Euclidian distance function was adopted as another criterion

$$NND = \sqrt{(1-NSE)^2 + (1-NSE_{ln})^2 + (Dv/100)^2} \qquad (10)$$

where NND is the Euclidian distance from the ideal point of NSE, NSE_{ln} and Dv. All the three components are dimensionless, and their ideal values are 1, 1, and 0, respectively. The smaller the NND is, the better the model performance will be. If the three components have different range or scale, weighting factors can be used for adjusting the emphasis on different components (Gupta et al., 2009).

The four criteria were also taken as objective functions in analyzing the effects of different objective functions on the SRM performances using the PSOA algorithm.

3.5. Comparison of the SOA and PSOA algorithms in snowmelt runoff simulation using SRM

The parameters of C_S and C_R were calibrated and the model performance was evaluated by using the calibration algorithms, SOA and PSOA, in the following procedure: Firstly, the SRM calibration for each snowmelt season from March to June during the 2001–2012 period was conducted separately using the two calibration algorithms, obtaining two optimal sets of C_S and C_R for each snowmelt season by both algorithms. Secondly, the long-term snowmelt runoff for all snowmelt seasons was simulated as a whole by the SRM model using both algorithms with a split-sample procedure (calibration and validation phases), only two sets of C_S and C_R were obtained by both algorithms during calibration phase. The enumeration approach was adopted in each step of both algorithms to search for optimal values of C_S and C_R from all possible combined sets of them within adjustment ranges. The initial runoff was set as follows: for the first sub-period, it was set to be the

observed streamflow of the day before the sub-period; for the following sub-periods, it is the simulated streamflow at the end of the previous sub-period. The effects of different lengths of sub-periods and objective functions on the model performance were also analyzed.

4. Results

4.1. The performance of the SOA and PSOA algorithms for the SRM calibration in each snowmelt season

To evaluate the performance of the PSOA algorithm in reference to the standard SOA algorithm, the calibration of snowmelt runoff for each snowmelt season during 2001–2012 was conducted with NSE as the objective function. The parameters C_S and C_R to be calibrated were allowed to vary within the range of 0.2 and 0.75 at a discrete size of 0.01 for each sub-period. The recession coefficient related parameters ρ and σ were calculated to be 1.076 and 0.055, respectively, based on the recession discharge data of the snowmelt seasons from 2001 to 2012 at the KSWT Station.

4.1.1. The statistics of the model performance

Tables 9 and 10 show the summary of the calibration results for 12-year snowmelt seasons in terms of NSE, NSE_{ln}, Dv and NND, respectively, using the two calibration methods with different sub-periods (i.e. one month, half a month, ten days, and five days). The variability of models' performance criteria using the two calibration methods is provided using box-and-whisker diagrams in Fig. 4.

It can be seen from Table 9 and Fig. 4(a) that for any given sub-period, the mean and standard deviation (SD) of NSE, obtained by PSOA are better than those by SOA. It is also seen that the mean, SD, and three quartiles of NSE by PSOA show continuous improvements when the length of sub-period becomes shorter. But this is not always the case by SOA.

Table 9 and Fig. 4(b) show the changes of NSE_{ln} with calibration sub-period. For most sub-periods, the mean of NSE_{ln} is improved using the PSOA method compared to the SOA method, although the maximized NSE does not guarantee a maximized NSE_{ln}. When the length of

Table 9
The 12-year means and SDs of NSE and NSE$_{ln}$ obtained for different lengths of sub-period by using the SOA and PSOA calibration methods. Im* indicates the relative increase by PSOA (%) for the same sub-period.

		NSE				NSE$_{ln}$			
		One month	Half a month	Ten days	Five days	One month	Half a month	Ten days	Five days
mean	SOA	0.850	0.871	0.871	0.863	0.913	0.913	0.923	0.895
	PSOA	0.854	0.883	0.894	0.907	0.904	0.920	0.925	0.929
Im* in mean		0.4	1.4	2.6	5.1	−1.0	0.7	0.2	2.8
SD	SOA	0.126	0.118	0.113	0.115	0.051	0.049	0.037	0.067
	PSOA	0.123	0.108	0.102	0.102	0.065	0.055	0.052	0.053
Im* in SD		2.4	8.5	9.7	11.3	−27.5	−12.3	−40.5	20.9

sub-period becomes shorter, the mean and three quartiles of NSE$_{ln}$ obtained by PSOA show a little bit of improvement. But those of NSE$_{ln}$ by SOA do not always improve and even deteriorate. Besides, the SDs obtained by PSOA reach a stable state when the length of sub-period becomes shorter, whereas SDs obtained by SOA are unstable, even though they are better than those by PSOA for some sub-periods.

Table 10 and Fig. 4(c) show the changes of Dv with calibration sub-periods. It can be seen that for a given sub-period, although NSE is selected to be maximized, the mean (the average of all absolute Dv values), SD and three quartiles of the simulated flow volumes are improved more obviously using PSOA than SOA. When the sub-period becomes shorter, the mean, SD and three quartiles of Dv obtained using the PSOA method also show a stable state, while those using the SOA method show an increasing trend.

Table 10 and Fig. 4 (d) show the changes of NND with calibration sub-periods. For a given sub-period, both mean and SD of the NND values are improved using the PSOA method compared to the SOA method, although NSE is maximized. Besides, the mean, SD and three quartiles of NND obtained by PSOA show improving trends when the length of sub-period becomes shorter, but those by SOA do not always improve and even deteriorate when the sub-period becomes shorter.

In conclusion, the statistics of the four criteria obtained by the PSOA method are better than those by the SOA method for a given sub-period. The statistics by PSOA show improving trend or stable state when the lenth of sub-period becomes shorter, but those by SOA do not always improve and even deteriorate.

4.1.2. Simulated daily runoff hydrographs

Fig. 5 shows the observed and simulated daily runoff hydrographs using the PSOA and SOA methods for each snowmelt season between 2001 and 2012 with a sub-period of five days. It can also be seen apparently from Fig. 5 that PSOA produced an overall better agreement with the observed runoff curve than SOA. The time of the simulated hydrograph peaks using PSOA and SOA is similar, but the peak values by PSOA match better to the observed values.

All results discussed in Section 4.1 show that the PSOA method performs better than the SOA method in parameter calibration.

4.2. The performance of the SOA and PSOA algorithms in long-term snowmelt runoff simulation using SRM

The long-term snowmelt runoff simulation using SRM was conducted for the snowmelt seasons of 2001–2012 by using the SOA and PSOA calibration algorithms. Model calibration was performed for the snowmelt seasons of 2001–2008 while validation was for 2009–2012. During calibration, NSE was selected as the objective function. C_S and C_R of zone A were both calibrated for the same sub-period for the snowmelt seasons of 2001–2008 (e.g. C_S or C_R have unique value for each snowmelt month of 2001–2008 taking one month as sub-period), which were also allowed to vary within the range of 0.20 and 0.75 at a discrete size of 0.01. The parameters ρ and σ that are related to recession coefficient during calibration and validation phases were calculated to be 1.086 and 0.059, respectively, using the recession discharge data of the snowmelt seasons from the calibration period (2001 to 2008) at the KSWT Station, assuming that they are unknown during validation phase.

4.2.1. Calibrated values of C_S and C_R using PSOA algorithm

Table 11 shows the calibrated C_S and C_R values from the PSOA calibration only, since the changing pattern of C_S and C_R values calculated from SOA was similar. It can be seen from the table that C_S value decreases from March to May, and then increases slightly in June, and C_R decreases from March to April, and then increases slightly in May and June for all lengths of sub-period, although there are some sudden jumps when the length of sub-period become short. From March to May, warmer temperatures result in higher snowmelt or rainfall losses from evaporation and infiltration, resulting in the decrease of C_S and C_R. Some sudden jumps in C_S and C_R may be caused by the model considering the varied hydrometeorological, snow cover ratio and soil moisture conditions in much more details when the length of sub-period become shorter.

4.2.2. The model performance in the calibration and validation phases using the SOA and PSOA algorithms

The average values of NSE, NSE$_{ln}$, Dv and NND from the calibration and validation phases with different sub-periods using the two calibration algorithms are shown in Figs. 6 and 7. It can be seen that the
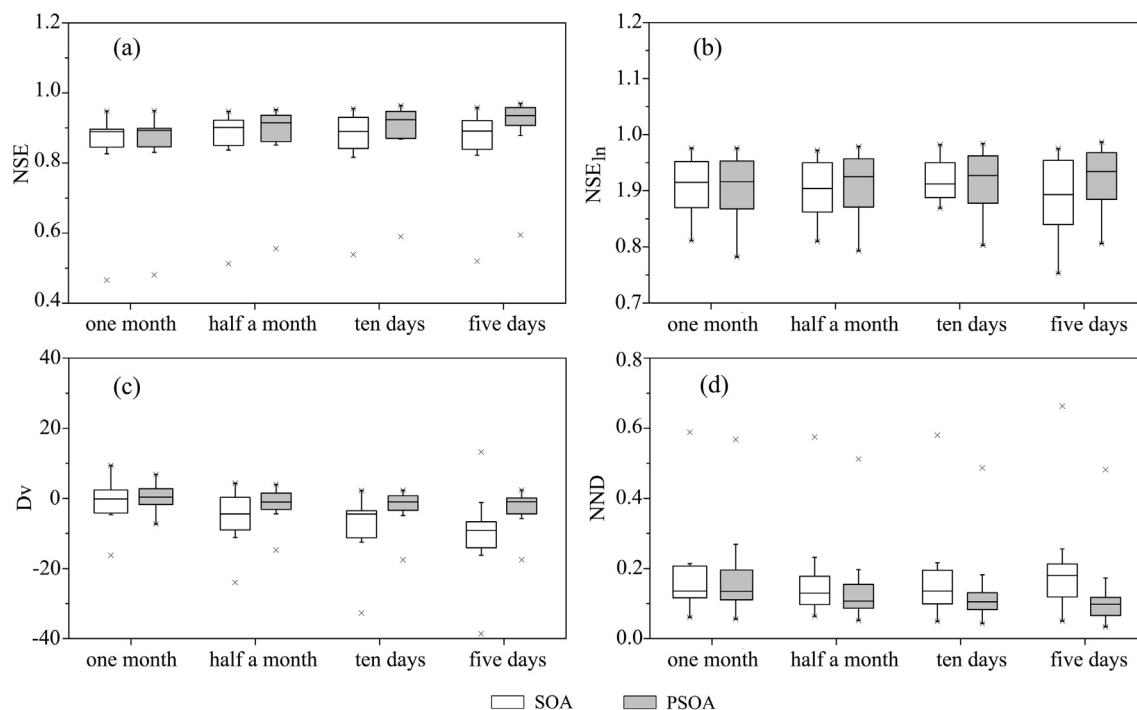
Table 10
The 12-year means and SDs of Dv and NND obtained for different lengths of sub-period by using the SOA and PSOA calibration methods. Im* indicates the relative increase by PSOA (%) for the same sub-period.

		Dv				NND			
		One month	Half a month	Ten days	Five days	One month	Half a month	Ten days	Five days
mean	SOA	4.52	6.25	7.66	11.86	0.183	0.174	0.176	0.217
	PSOA	3.18	3.09	3.24	3.16	0.182	0.149	0.139	0.127
Im* in mean		29.6	50.6	57.7	73.4	0.6	14.4	21.0	41.5
SD	SOA	6.47	7.81	9.30	11.94	0.138	0.135	0.137	0.153
	PSOA	4.05	4.86	5.31	5.23	0.135	0.122	0.116	0.118
Im* in SD		37.4	29.7	42.9	56.2	2.2	9.6	15.3	22.9

Fig. 4. Variabilities with calibration sub-periods of NSE (a), NSE$_{ln}$ (b), Dv (c) and NND (d) values calculated using the two calibration algorithms over the 12 snowmelt seasons (2001–2012).

average NSE values obtained using PSOA are larger than those using SOA for all sub-periods in both the calibration and validation phases. The average values of NSE$_{ln}$, Dv and NND are also improved using the PSOA method in both the calibration and validation phases. It can also be seen that during the calibration phase the average values of NSE, NSE$_{ln}$, and NND obtained using the PSOA method show increasing trends of improvements when the length of sub-period decreases, while there is no such trend using the SOA method. Besides, NSE, NSE$_{ln}$, and NND improve more using PSOA than SOA when the length of sub-period is reduced. All the results indicate that PSOA is more robust than SOA, and suggest the superiority of PSOA to SOA, especially when the sub-period is short.

4.3. Effects of different objective functions and sub-periods on model performance

The results of the average values of NSE, NSE$_{ln}$, DV, and NND for various sub-periods and different objective functions are shown in Figs. 8 and 9 for the calibration and validation phase, respectively. It is seen that different objective functions result in similar model performance in both the calibration and the validation phases for a given sub-period, except for the objective function Dv, which results in an apparently worse performance for the sub-period of five days.

The impacts of the sub-period length on model performance for different objective functions are complex. Taking all the four evaluation criteria into consideration, during the calibration phase the model performance is improved continually when the length of sub-period becomes shorter for any objective function except for the Dv. However, in the validation phase there is no improvement or any other varying patterns when the length of sub-period is getting shorter. This phenomenon is probably due to over fitting, over fitted simulation in the calibration phase leads to poor prediction in the validation phase. Thefore, a compromised length of sub-period and objective function may have to be chosen as a trade-off among evaluation criteria and between the importance of calibration and validation phases based on the objective of the model application.

Generally, Dv, which is usually used as a criterion of model

performance focusing on volumes, was not recommended to take as the objective function for dynamic streamflow prediction because its weakness in accounting for the day-to-day difference between observed and simulated discharge. Hence, it is thus expected that the model with Dv as an objective function shows unstable performance for different lengths of sub-period in this case study.

5. Discussions

The hydrological processes and precipitation-runoff relationship are generally complex, which change not only within years or decades, but also in seasons. To capture the time-varying nature of hydrological processes and reduce model uncertainty it is necessary to allow key parameters of hydrological models varying with time during model calibration and validation stages (Levesque et al., 2008; Zhang et al., 2011; Kim and Lee 2014; Kim 2016). A most approachable method is to divide the hydrological year into several sub-periods, and assume that the model parameters are constant in each sub-period. This approach is equivalent to approximating a smooth curve in time with a function of steps. The smaller the sub-periods are, the better the approximation will be. Both the SOA and PSOA algorithms are such approaches. Obviously they are not perfect but both are at least better than taking the model parameters as constant during the whole calibration period while they are in fact variable. It should be noted that the selection of parameters to be optimized is important. The selected parameters must be time variant, and a certain jump in parameter values between two adjacent sub-periods is tolerable. Generally, constant parameter such as maximum capacity of soil storage can not be optimized in each sub-period. If such a parameter is optimized sub-period by sub-period, continuity problems in the water balance will occur when the parameter value changes from one sub-period to the next. For instance, if the capacity is 100 mm and the content in the store is 90 mm at the end of the first period, and the capacity on the next period is 80 mm, what is done with the 10 mm over the capacity? Therefore, the selection of parameters to be optimized must be done with due care, when applying a calibration algorithm such as SOA and PSOA. There are two ways to partition the whole data period into sub-periods, one is dividing the observation data
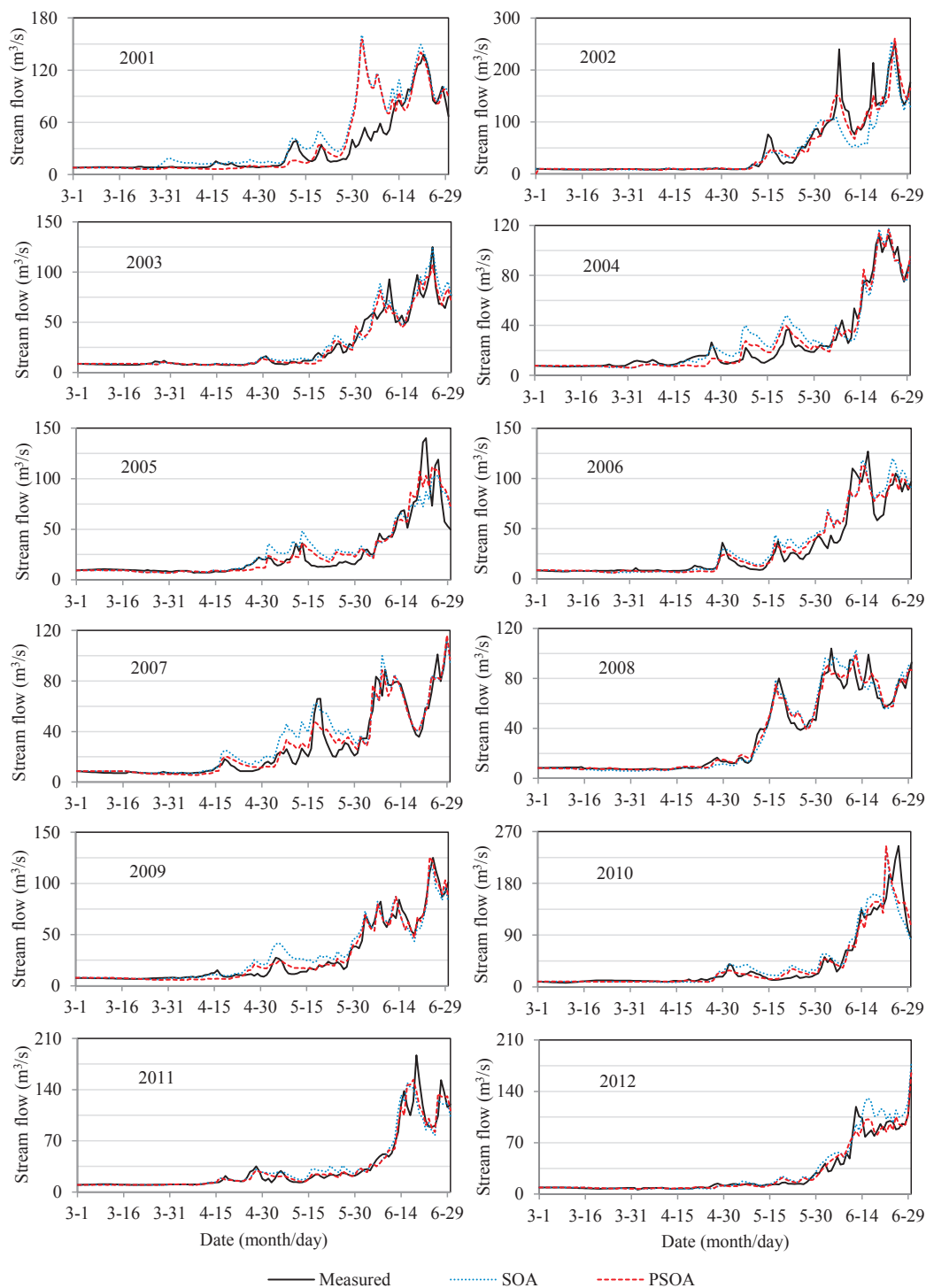
Fig. 5. The observed and calculated daily runoff hydrographs with a sub-period of five days.

into several periods of hydroclimatic similarity; the other way is to directly divide the calibration period into several sub-periods with the same length. In the second way, extensive efforts on classifying the whole calibration period into too many sub-periods with different lengths based on hydro-meteorological characteristics can be avoided.

Generally, the evaluation criteria such as NSE, NSE_{ln} and Dv will get improvement when the length of sub-period becomes shorter using calibration method such as the PSOA algorithm. This is the situation in calibration phase in our case study, however, in the validation phase, the criteria do not always improve accordingly, resulting in overfitting problems, which indicates that the model does not always produce

better performance with too short sub-periods in the validation phase. Such overfitting problems are not caused by calibration algorithm itself, but probably by factors such as the structure of the hydrological model used, non-stationarity of the snowmelt runoff process between the calibration and validation phases, lack of 'power' in the objective function, etc. (Gupta et al., 2009). Other important factors may include that the model considers the hydrological characteristics with too many details when a too short sub-period is adopted in the calibration phase. A short sub-period increases the number of calibrated parameters and makes these parameters vary irregularly (see Table 11), leading to poor performance in validation phase. Hence, a compromised sub-period

Table 11
Calibrated values of C_S and C_R using PSOA (2001–2008).

Sub-period	One Month		Half a month		Ten days		Five days	
	C_S	C_R	C_S	C_R	C_S	C_R	C_S	C_R
March	0.470	0.750	0.750	0.750	0.750	0.750	0.750	0.200
							0.750	0.750
					0.750	0.750	0.750	0.200
			0.340	0.750			0.410	0.750
					0.320	0.750	0.750	0.750
							0.230	0.690
April	0.260	0.200	0.290	0.200	0.320	0.420	0.350	0.390
							0.200	0.200
					0.260	0.200	0.330	0.200
			0.200	0.200			0.200	0.200
					0.200	0.200	0.200	0.200
							0.200	0.200
May	0.200	0.240	0.390	0.200	0.200	0.200	0.200	0.200
							0.200	0.200
					0.300	0.200	0.570	0.200
			0.200	0.260			0.200	0.200
					0.200	0.290	0.300	0.200
							0.200	0.470
June	0.290	0.290	0.200	0.340	0.200	0.360	0.200	0.340
							0.200	0.320
					0.520	0.200	0.700	0.200
			0.440	0.200			0.430	0.200
					0.390	0.200	0.430	0.200
							0.330	0.200

should be chosen as a trade-off between the importance of calibration and validation.

There are many factors affecting the model performance: the quality of the observed data as inputs, the accuracy of the values of the non-calibrated parameters, and accuracy of the calibrated model parameters. For SRM, the important model inputs are the fraction of snow covered area, the precipitation (snow or rain), air temperature data, and the number of elevation zones. The model's key parameters include the runoff coefficients of snowmelt and rainfall, the degree-day factor, and the temperature lapse rate. In the present study, although only two model parameters, i.e., the runoff coefficients of snowmelt and rainfall, were calibrated, there is no limit of the number of parameters to be calibrated in the calibration methods such as PSOA and SOA

themselves. However, the more parameters to be calibrated is, the more difficult it is to obtain their optimal values and to evaluate them on short sequences. For the current case study on the Manasi River basin, due to spare hydro-meteorological stations, input data such as precipitation for each zone were estimated based on the observed records and corrected TRMM data for the same study area. Some model parameters were predetermined based on the references (Xu, 1996; Feng et al., 2000; Hu, 2004), and the time variant parameters such as the temperature lapse rate and the mass density of snow only were allowed to change monthly. If daily temperature and precipitation are obtained directly from new data sources such as MODIS and TRMM, or the temperature lapse rate and the mass density of snow are allowed to change with different length of sub-periods, and more elevation zones are considered, the model performance using PSOA might be different.

In this study, all results show that the proposed new calibration algorithm (PSOA) outperforms the SOA algorithm. Detailed comparison with SOA showed that the model performance is better than SOA for both single-snowmelt-season and multi-snowmelt-season simulations in terms of NSE, NSEln, Dv and NND. The improvement of model performance using PSOA over SOA for calibration should be generally true, but the extent of the improvement by PSOA over SOA is expected to depend on a basin's characteristics, the model structure, the quality of input data, the values of non-calibrated parameters, and sub-period length for calibration. A further research on the performance of PSOA in different basins would need to be carried out.

6. Summary and conclusions

In this study we proposed a progressive segmented optimization algorism (PSOA) for calibrating time-variant parameters of hydrological models. The algorithm was applied to simulate snowmelt runoff during the snowmelt seasons of 2001–2012 taking the Manas River basin of Xinjiang, China as a test site using the SRM model. The PSOA and standard SOA algorithms were compared and evaluated for both single-snowmelt-season calibration and multi-snowmelt-season simulation (2001–2008 as the calibration phase and 2009–2012 as the validation phase). The effects of objective functions and sub-period length on model performance have also been analyzed. The study concluded that:

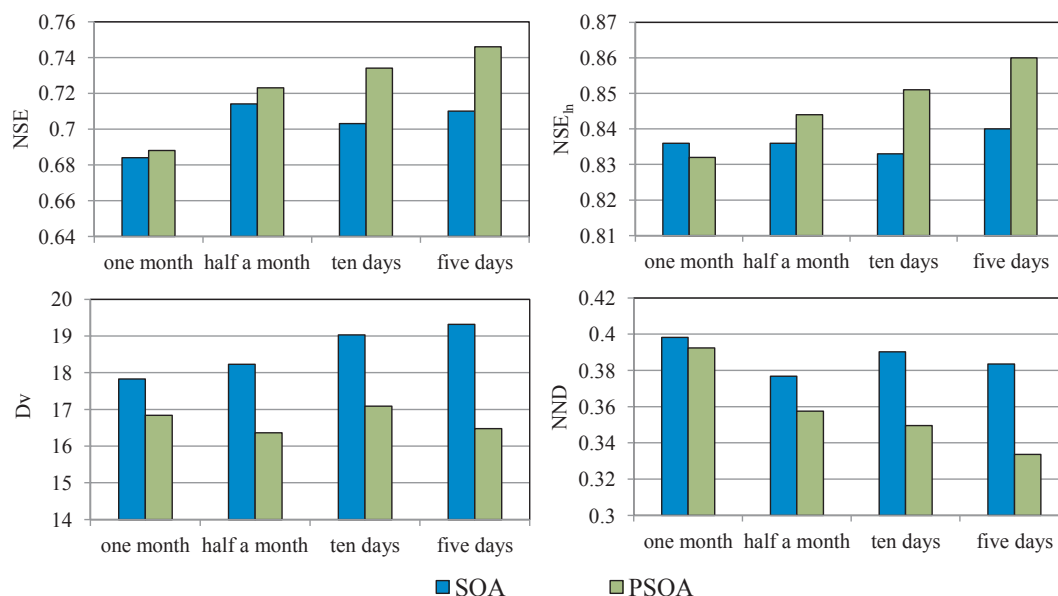1) PSOA can effectively calibrate the time-variant model parameters

Fig. 6. The average values of NSE (the upper left), NSE$_{ln}$ (the upper right), Dv (the bottom left) and NND (the bottom right) versus the sub-period during the calibration phase (2001–2008) calculated from the SRM model using the SOA and PSOA algorithms.
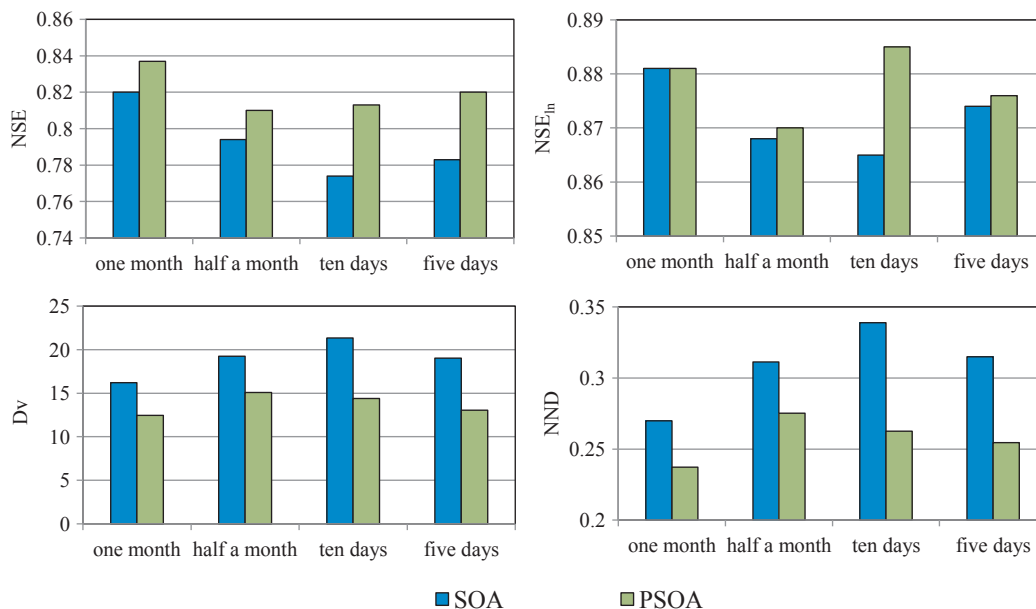
Fig. 7. The average values of NSE (the upper left), NSE_{ln} (the upper right), Dv (the bottom left) and NND (the bottom right) versus the sub-period during the validation phase (2009–2012) calculated from the SRM model.

while avoiding too much computational time caused by a significant increase of parameter dimensionality.

2) For any given sub-period, PSOA outperforms SOA in terms of NSE, NSE_{ln}, Dv, and NND both in the model calibration of single-snowmelt-season and in multi-snowmelt-season simulation for both calibration and validation periods, as SOA seeks optimal parameters for the sub-period by optimizing the objective function based on the measured and estimated data only in the same sub-period, while PSOA seeks optimal parameters by optimizing the objective function based on both the current and all the prior sub-periods.

3) For single-snowmelt-season calibration, the length of the sub-period has apparent effect on model performance, the shorter the sub-period is, the better the model performance will be when the model is calibrated using the PSOA method.

4) In multi-snowmelt-season simulation using the PSOA algorithm, the model performances have little difference in all evaluation criteria

when NSE, NSE_{ln}, and NND are used as the objective functions, but much better than the case when Dv is used as the objective function, especially for the sub-period of five days.

5) For multi-snowmelt-season simulation, too short sub-periods may cause overfitting problems when selecting some functions as objectives. A compromised length of sub-period may have to be chosen as a trade-off between the importance of calibration and validation in such a case.

The proposed PSOA method in the present study can be adopted for multi-snowmelt-season calibration, which can identify more effective parameter set, and improve model performance. Besides, the idea of the PSOA method can be beneficial for multi-period optimization searching for global optimal solution. According to the principle of the PSOA algorithm, it can be used for multi-snowmelt-season calibration not only for a single length of sub-period but also for different lengths of
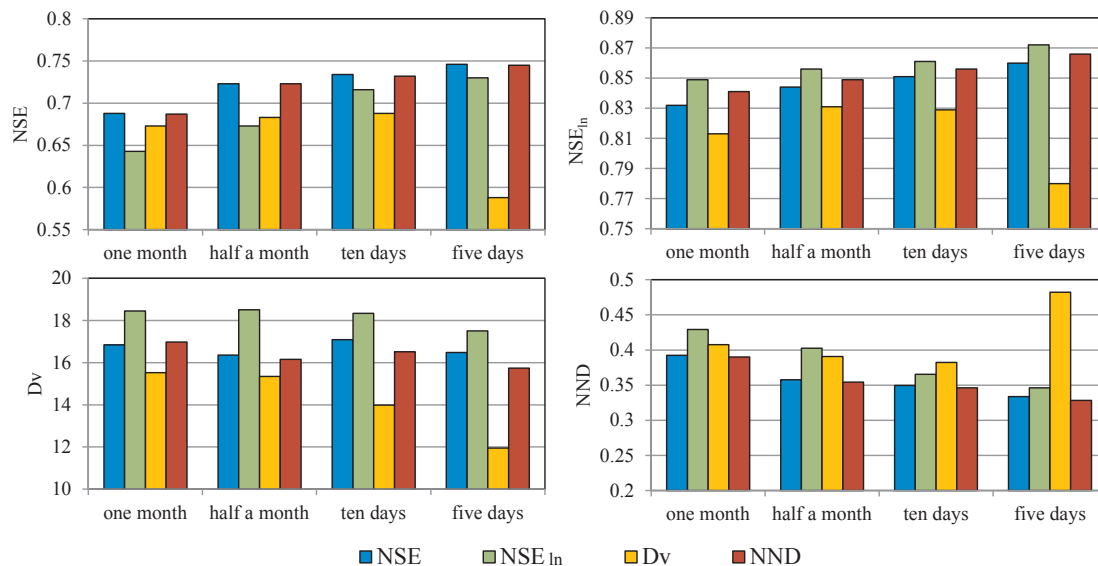

Fig. 8. The average values of NSE (the upper left), NSE_{ln} (the upper right), Dv (the bottom left) and NND (the bottom right) versus the sub-period for different objective functions (NSE, NSE_{ln}, Dv, and NND) during the calibration phase (2001–2008), where the model calibration was performed using the PSOA method.
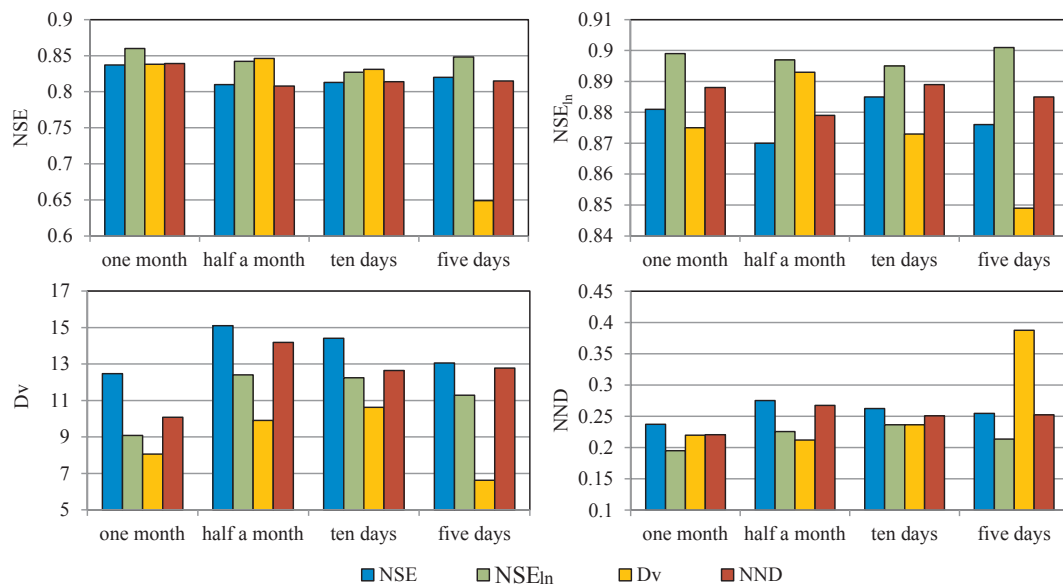
Fig. 9. The average values of NSE (the upper left), NSE_{ln} (the upper right), Dv (the bottom left) and NND (the bottom right) versus the sub-period for different objective functions (NSE, NSE_{ln}, Dv, and NND) during the validation phase (2009–2012).

sub-period in order to better capture the time varying nature of the hydrological process at variant time scales.

Acknowledgements

References

Beven, K., Binley, A., 1992. The future of distributed models-model calibration and uncertainty prediction. Hydrol. Process. 6, 279–298.

Beighley, R.E., Moglen, G.E., 2002. Trend assessment in rainfall-runoff behavior in urbanizing watersheds. J. Hydrol. Eng. 7 (1), 27–34.

Boyle, D.P., Gupta, H.V., Sorooshian, S., 2000. Toward improved calibration of hydrologic models: combining the strengths of manual and automatic methods. Water Resour. Res. 36. https://doi.org/10.1029/2000wr900207.

Butt, M.J., Bilal, M., 2011. Application of snowmelt runoff model for water resource management. Hydrol. Process. 25 (24), 3735–3747.

Chen, Y., Chen, X., Xu, C., Zhang, M., Liu, M., Gao, L., 2018. Toward improved calibration of SWAT using season-based multi-objective optimization: a case study in the Jinjiang Basin in Southeastern China. Water Resour. Manage. 32, 1193–1207.

Choi, H.T., Beven, K., 2007. Multi-period and multi-criteria model conditioning to reduce prediction uncertainty in an application of TOPMODEL within the GLUE framework. J. Hydrol. 332, 316–336.

de Vos, N.J., Rientjes, T.H.M., Gupta, H.V., 2010. Diagnostic evaluation of conceptual rainfall-runoff models using temporal clustering. Hydrol. Process. 24 (20), 2840–2850.

Farr, T.G., Rosen, P.A., Caro, E., Crippen, R., Duren, R., Hnseley, S., Kobrick, M., Paller, M., Rodriguez, E., Roth, L., Seal, D., Shaffer, S., Shimada, J., Umland, J., Werner, M., Oskin, M., Burbank, D., Alsdorf, D., 2007. The shuttle radar topography mission. Rev. Geophys. 45 (2). https://doi.org/10.1029/2005RG000183.

Feng, X., Li, W., Shi, Z., Wang, L., 2000. Satellite snow cover monitoring and snowmelt runoff simulation of Manas river in Tianshan region. Remote SNSE. Tech. App. 15 (1), 18–21 (in Chinese).

Georgievsky, M.V., 2009. Application of the snowmelt runoff model in the kuban river basin using MODIS satellite images. Environ. Res. Lett. 4 (4), 045017.

Gupta, H.V., Kling, H., Yilmaz, K.K., Martinez, G.F., 2009. Decomposition of the mean squared error and NSE performance criteria: Implications for improving hydrological modeling. J. Hydrol. 377, 80–91.

Gupta, H.V., Sorooshian, S., Yapo, P.O., 1998. Toward improved calibration of hydrologic models: multiple and non-commensurable measures of information. Water Resour. Res. 34. https://doi.org/10.1029/97wr03495.

Gupta, V.K., Sorooshian, S., 1983. Uniqueness and observability of conceptual rainfall-runoff model parameters: The percolation process examined. Water Resour. Res. 19, 269–276.

Hao, L., Sun, G., Liu, Y., Wan, J., Qin, M., Qian, H., Liu, C., Zheng, J., John, R., Fan, P., Chen, J., 2015. Urbanization dramatically altered the water balances of a paddy field-dominated basin in southern China. Hydrol. Earth Syst. Sci. 19, 3319–3331.

Hay, L.E., McCabe, G.J., Clark, M.P., Risley, J.C., 2009. Reducing streamflow forecast uncertainty: application and qualitative assessment of the Upper Klamath River Basin. Oregon. J. Amer. Water Resour. Assoc. 45, 580–596.

Hu, R.J., 2004. Physical Geography of the Tianshan Mountain in China. China Environmental Science Press, Beijing (in Chinese).

Huang, X., Zhang, X., Li, X., Liang, T., 2007. Accuracy analysis for MODIS snow products of MOD10A1 and MOD10A2 in northern xinjiang area. J. Glaciol. Geocryol. 29, 722–729 (in Chinese).

Immerzeel, W.W., Droogers, P., de Jong, S.M., Bierkens, M.F.P., 2009. Large-scale monitoring of snow cover and runoff simulation in Himalayan river basins using remote sensing. Remote Sens. Environ. 113 (1), 40–49.

Ji, X., Chen, Y.F., 2012. Characterizing spatial patterns of precipitation based on corrected TRMM 3B43 data over the Mid Tianshan Mountains of China. J. Mt. Sci. 9, 628–645.

Jie, M.X., Chen, H., Xu, C.-Y., Zeng, Q., Tao, X.E., 2016. A comparative study of different objective functions to improve the flood forecasting accuracy. Hydrol. Res. 47 (4), 718–735. https://doi.org/10.2166/nh.2015.078.

Kim, H.S., Lee, S., 2014. Assessment of a seasonal calibration technique using multiple objectives in rainfall–runoff analysis. Hydrol. Process. 28, 2159–2173.

Kim, H.S., 2016. Potential improvement of the parameter identifiability in ungauged catchments. Water Resour. Manag. 30 (9), 3207–3228.

Kult, J., Choi, W., Choi, J., 2014. Sensitivity of the Snowmelt Runoff Model to snow covered area and temperature inputs. Appl. Geogr. 55, 30–38.

Levesque, E., Anctil, F., van Griensven, A., Beauchamp, N., 2008. Evaluation of streamflow simulation by SWAT model for two small watersheds under snowmelt and rainfall. Hydrol. Sci. J. 53, 961–976.

Madsen, H., 2000. Automatic calibration of a conceptual rainfall-runoff model using multiple objectives. J. Hydrol. 235, 276–288.

Martinec, J., 1975. Snowmelt-runoff model for stream flow forecasts. Nordic Hydrol. 6 (3), 145–154.

Martinec, J., Rango, A., 1986. Parameter values for snowmelt runoff modelling. J. Hydrol. 84, 197–219.

Martinec, J., Rango, A., Roberts, R.T., 2008. Snowmelt Runoff Model (SRM) User's Manual, 19–39. New Mexico State University Press, New Mexico.

Merz, R., Blöschl, G., Parajka, J., 2006. Spatio-temporal variability of event runoff coefficients. J. Hydrol. 331, 591–604.

Nash, J.E., Sutcliffe, J.V., 1970. River flow forecasting through conceptual models part I – A discussion of principles. J. Hydrol. 10 (3), 282–290.

Paik, K., Kim, J.H., Kim, H.S., Lee, D.R., 2005. A conceptual rainfall-runoff model considering seasonal variation. Hydrol. Process. 19, 3837–3850.

Qiu, L., You, J., Qiao, F., Peng, D., 2013. Simulation of snowmelt runoff in ungauged basins based on MODIS: a case study in the Lhasa River basin. Stoch. Env. Res. Risk A. https://doi.org/10.1007/s00477-013-0837-4.

Shamir, E., Imam, B., Gupta, H.V., Sorooshian, S., 2005. Application of temporal streamflow descriptors in hydrologic model parameter estimation. Water Resour. Res. 41, W06021. https://doi.org/10.1029/2004WR003409.

Tahir, A.A., Chevallier, P., Arnaud, Y., Neppel, L., Ahmad, B., 2011. Modeling snowmelt-runoff under climate scenarios in the Hunza River Basin, Karakoram Range, northern

Pakistan. J. Hydrol. 409 (1–2), 104–117.

Toth, E., 2009. Classification of hydro-meteorological conditions and multiple artificial neural networks for streamflow forecasting. Hydrol. Earth Syst. Sci. 13, 1555–1566.

Tian, F., Li, H., Sivapalan, M., 2012. Model diagnostic analysis of seasonal switching of runoff generation mechanisms in the blue River Basin. Oklahoma. J. Hydrol. 418–419, 136–149.

Vrugt, J.A., Gupta, H.V., Bastidas, L.A., Bouten, W., Sorooshian, S., 2003. Effective and efficient algorithm for multiobjective optimization of hydrologic models. Water Resour. Res. 39, 1214. https://doi.org/10.1029/2002WR001746.

Xu, J., 1996. Initial meteorological conditions for the formation of stable snow cover in the Tianshan Mountains area. Arid Land Geogr. 19 (4), 51–55 (in Chinese).

Yapo, P.O., Gupta, H.V., Sorooshian, S., 1998. Multi-objective global optimization for hydrologic models. J. Hydrol. 204 (1–4), 83–97.

Zhang, D.J., Chen, X.W., Yao, H.X., Lin, B.Q., 2015a. Improved calibration scheme of

SWAT by separating wet and dry seasons. Ecol. Model. 301, 54–61.

Zhang, H., Huang, G.H., Wang, D.L., Zhang, X.D., 2011. Multi-period calibration of a semi-distributed hydrological model based on hydroclimatic clustering. Adv. Water Resour. 34, 1292–1303.

Zhang, F., Zhang, H., Hagen, S.C., Ye, M., Wang, D., Gui, D., Zeng, C., Tian, L., Liu, J., 2015b. Snow cover and runoff modelling in a high mountain catchment with scarce data: effects of temperature and precipitation parameters. Hydrol. Process. 29, 52–65.

Zhou, J., Ouyang, S., Wang, X., Ye, L., Wang, H., 2014. Multi-objective parameter calibration and multi-attribute decision-making: an applicationto conceptual hydrological model calibration. Water Resour. Manage. 28, 767–783.

Zhou, X., Xie, H., Hendrickx, J.M.H., 2005. Statistical evaluation of remotely sensed snow-cover products with constraints from streamflow and SNOTEL measurements. Remote Sens. Environ. 94, 214–231.